Adsorption of carcinogenic dye Congo red onto prepared graphene oxide-based composites

Alaa A. Mizhir[a], Ali A. Abdulwahid[b], Hadi S. Al-Lami[b],*

[a]*Department of Applied Marine Science, Faculty of Marine Science, University of Basrah, Basrah, Iraq, Tel. +964 782 532 0622; email: albahily79@yahoo.com (A.A. Mizhir)*
[b]*Department of Chemistry, College of Science, University of Basrah, Basrah, Iraq, Tel. +964 770 737 7488; email: hadisalman54@yahoo.com (H.S. Al-Lami), Tel. +964 780 140 0141; email: alirazaq2013@yahoo.com (A.A. Abdulwahid)*

ABSTRACT

Graphene oxide (GO), graphene oxide/chitosan (GOCS), and graphene oxide/poly(*n*-butyl methacrylate-co-methacrylic acid) (GOpBCM) composites were prepared as adsorbents for removal of carcinogenic dye Congo red (CR) from aqueous solutions. They were characterized by various techniques, including Fourier-transform infrared spectroscopy, field emission scanning electron microscopy, and X-ray diffraction spectroscopy. Adsorption equilibrium isotherms, adsorption kinetics and thermodynamic studies of the batch adsorption process were done to evaluate the fundamental adsorption properties of the dye CR. The results indicate that the adsorption of CR on the adsorbents was high pH and temperature-dependent. The maximum adsorption of 1,666 mg/g occurred at pH 3.0 for an initial dye concentration of 500.0 mg/L by GOCS, whereas, the maximum adsorption obtained from an initial dye concentration 300.0 mg/L was 1,000 mg/g for GO and GOpBCM at pH 3.0 and 7.0 respectively. The experimental equilibrium adsorption data were explored by three different two-parameter models Langmuir, Freundlich and Temkin isotherms. The Langmuir model was well agreed with experimental data for all adsorbents. The kinetic models, namely pseudo-first-order, pseudo-second-order, and intraparticle-diffusion are employed to understand the mechanism of the adsorption process, and it fitted very well the pseudo-second-order kinetic model for all adsorbents. The calculated thermodynamic parameters revealed that the adsorption is a spontaneous and endothermic process.

Keywords: Graphene oxide; Grafting; Composites; Adsorption isotherm; Congo red; Pseudo-second-order

1. Introduction

Nowadays, the widespread use of harmful chemical compounds and some hazardous materials around the world has led to severe water contamination, especially with most industrial dyes, some heavy metal ions, and other very toxic molecules, which may lead to retention toxicities, lethal poisoning and carcinogenic contact with human beings and animals even at ultralow concentrations [1].

These days, many printing and dyeing industries make use of hydrocarbons like naphthalene, benzene, xylene, anthracene, etc. to prepare a variety of dyes. These industries discharge processed solutions to the surface water without appropriate treatment resulting in the deterioration of water quality. The environment and human health are greatly affected due to water contamination by the presence of waste dyes [2,3]. Congo red (CR), an anionic dye, has been known to cause an allergic reaction and to be metabolized to benzidine, a human carcinogen [4,5].

* Corresponding author.

At present, the commonly used methods for treating CR-containing wastewater from printing and dye mainly include flocculation [6], chemical oxidation [7], biological degradation [8], and photocatalytic degradation [9–11]. However, all of these techniques suffer from one or more limitations. These techniques are either expensive, tedious, or generate highly harmful waste, and it is making the requirement of a cost-effective and environmentally friendly process, an essential need of the hour. During recent years, adsorption has gathered a great deal of consideration as a result of its simplicity, ease of operation, financial sustainability and accessibility of an extensive variety of adsorbents [3].

Various natural by-products, composite material as well as photocatalysts have been used in the past for the removal of dyes from contaminated water. Graphene oxide (GO) consisting of monolayer structure with oxygen functional groups, such as carboxyl, hydroxyl, and epoxy groups, is one of the most important derivatives of graphene [12]. The single-layer structure endows GO sheets with large specific surface area and highly negative-charged surface, which invests GO as an ideal candidate as the nanocarriers such as the drugs, genes, and other molecules [13,14]. GO can interact with many functional polymers containing abundant functional groups such as carboxyl and amino groups and adsorb pollutants through electrostatic interaction or chelation [15]. Although much effort has been devoted to the fabrication and characterization of graphene or graphene oxide-polymer composites, most of the attempts focused on their mechanical and electrical performance instead of the adsorptive property in wastewater treatments [16,17].

The role of polymers in most GO-polymer composites reported was usually to strengthen the mechanical property of the composites [18,19]. Among the limited studies on polymer-modified graphene oxide targeting the removal of dyes, chitosan has been chosen as functional polymers for eliminating some of the dyes from wastewater [20]. Functionalization of GO composites using polymers containing abundant carboxylic groups like poly(acrylic acid) and other analog polymers, which have a strong affinity to most positively charged organic pollutants and the ability to enhance water dispersibility has not been reported [21]. Recently, numerous researches have been carried out to explore the environmental applications of GO and GO-based composite adsorbents, and these composite materials revealed outstanding adsorption capacities against various toxic compounds in aqueous solution [22–24].

Water treatment is not deprived of using easy extracted natural or any prepared polymers. In this study, two new composites based on graphene oxide (GO) will be synthesized, namely graphene oxide-g-chitosan (GOCS) and graphene oxide-g-poly(*n*-butyl methacrylate-co-methacrylic acid) (GOpBCM). The objective of this study is to investigate the practicability of using the prepared composites for the removal of CR, a toxic dye, from wastewater by adsorption method. This present research work will explore the mechanism of adsorption and adsorption kinetics of the dye, and determine the various physicochemical controlling factors on the rate of adsorption and also on the capacity of the adsorbent. The adsorption isotherms will describe by using Langmuir, Freundlich, and Temkin isotherms. Further, this paper also discusses various thermodynamic parameters such as Gibbs free energy change ($\Delta G°$), the heat of adsorption ($\Delta H°$) and entropy change ($\Delta S°$) respectively. Finally, desorption study is important to clarify the reusability of the prepared adsorbents and to understand the nature of adsorption system and evaluate the ability of recycling.

2. Experimental setup

2.1. Materials and measurements

Natural graphite with a purity of 99.99% from Hopkin & Williams Co. Ltd., (UK). Chitosan with 80 mesh with a degree of deacetylation (75%–85%) from Merck (Germany), concentrated sulfuric acid (H_2SO_4), sodium nitrate and sodium chlorate ($NaNO_3$ and $NaClO_4$), potassium permanganate ($KMnO_4$), hydrogen peroxide (H_2O_2, 30%), hydrochloric acid (HCl, 36%), sodium hydroxide (NaOH), N,N'-dicyclohexylcarbodiimide (DCC), *n*-butyl-methacrylate monomer (BM), methacrylic acid (MAA), methanol (CH_3OH), benzoyl peroxide (used as initiator without further treatment) and 1-ethyl-3-(3-dimethylaminopropyl)carbodiimide hydrochloride (EDC) were purchased from Sigma-Aldrich Company (Germany). All other reagents used in this study were analytical grade and distilled, or double-distilled water was used in the preparation of all solutions.

Fourier-transform infrared spectroscopy (FTIR) of the prepared adsorbents were recorded by FTIR-8101M Shimadzu spectrometer (Japan) with KBr pellet in the region (400–4,000 cm^{-1}) to investigate the chemical structures. Adsorbents structure and morphology were identified using an FEI NOVA NanoSEM 450 (Netherland) field emission scanning electron microscopy (FESEM) under vacuum at an operating voltage of 10 kV. Patterns of X-ray diffraction (XRD) of the materials were recorded by a Rigaku X-ray powder diffraction diffractometer (Japan) using Cu K$_\alpha$ radiation with a wavelength of 1.54 Å at a scanning speed of 2 min^{-1} from 5° to 80°. The concentration of CR dye was measured in a quartz cell of 1 cm length at λ_{max} 494 nm using a Sentry 20 UV-Visible spectrophotometer model T180 (UK).

2.2. Synthesis of graphene oxide (GO)

Modified Hummers method for synthesis graphene oxide was carried out [25]. This was included dissolving 2.0 g of graphite and 1.0 g of $NaNO_3$ in 46.0 ml of concentrated H_2SO_4 under an ice bath. After about 15 min of stirring, 6.0 g of $KMnO_4$ was gradually added into the suspension with stirring as slowly as possible to control the reaction temperature below 20°C. The suspension was stirred for 2 h and then maintained at 35°C for 30 min. 100.0 mL of deionized water was slowly poured into the suspension, resulting in a quick increase in temperature, and the temperature should be controlled lower than 98°C. After 15 min, the suspension was then further diluted to approximately 280.0 ml with warm deionized water. 20.0 ml of 30% H_2O_2 was added to remove the residual $KMnO_4$ and MnO_2 to change the color into luminous yellow. Then, the suspension was filtered and washed with a warm 5% aqueous HCl aqueous solution and deionized water, respectively, until no sulfates were detected, and the pH of the filtrate was adjusted to 7. The sample of graphene oxide was dried under vacuum at 50°C to a constant weight.

2.3. Copolymerization of n-butyl methacrylate/methacrylic acid (pBCM)

BM monomer was washed twice with 5% NaOH to remove inhibitor and twice with water, then it was dried over anhydrous MgSO$_4$, then with calcium hydride, and freshly vacuum distilled before copolymerization. MAA was distilled under reduced pressure before use in the copolymerization using Bz$_2$O$_2$ as initiator.

The copolymerization was carried out in the round bottom flask of equimolar amounts of freshly distilled *n*-butyl methacrylate and methacrylic acid under dry N$_2$ gas in a water bath after adding benzoyl peroxide (1×10^{-4} mol/L) at 70° [26,27]. The copolymer was precipitated into methanol. It was filtered and washed several times with methanol and vacuum dried at room temperature.

2.4. Polymerization of graphene oxide-g-chitosan (GOCS)

GOCS was prepared according to the literature with some modifications [28] (Fig. 1). GO (0.5 g) was dispersed in 50.0 mL distilled water by ultrasonic dispersion for 3 h. A solution of 0.05 M DCC (0.0478 g) was added to the GO dispersion and stirring continuously for 2 h to activate the carboxyl groups of GO [29]. The pH of the solution was adjusted to 7 by 2% (w/v) NaOH solution. And then, the activated GO solution and 5 g CS were dispersed in 50 mL distilled water by ultrasonic dispersion for 20 min. After that, the mixed solutions were stirred at 60°C for 3 h. The precipitate was washed with NaOH solution and deionized water in turn until the pH was about 7. The obtained product GOCS was dried in a vacuum oven.

2.5. Polymerization of graphene oxide-g-poly(n-butyl methacrylate-co-methacrylic acid) (GOpBCM)

The route of the synthesis of GOpBCM) is presented in Fig. 2. GO (0.3 g) was dispersed in (7.5 mL) of phosphate buffer solution (pH 6) and ultra-sonicated for (30 min). pBCM (0.3 g) and EDC (0.03 g) were added to the GO dispersion, and the reaction mixture was sonicated for (30 min).
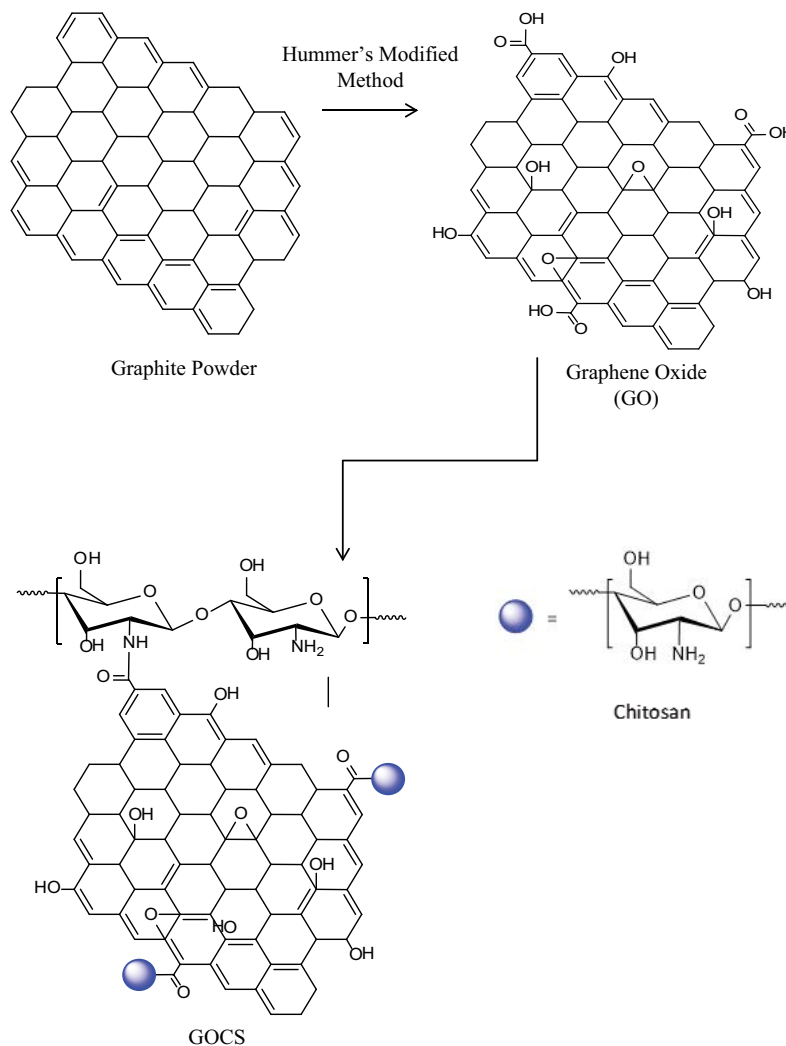

Fig. 1. Synthetic routes of preparing GOCS composite.
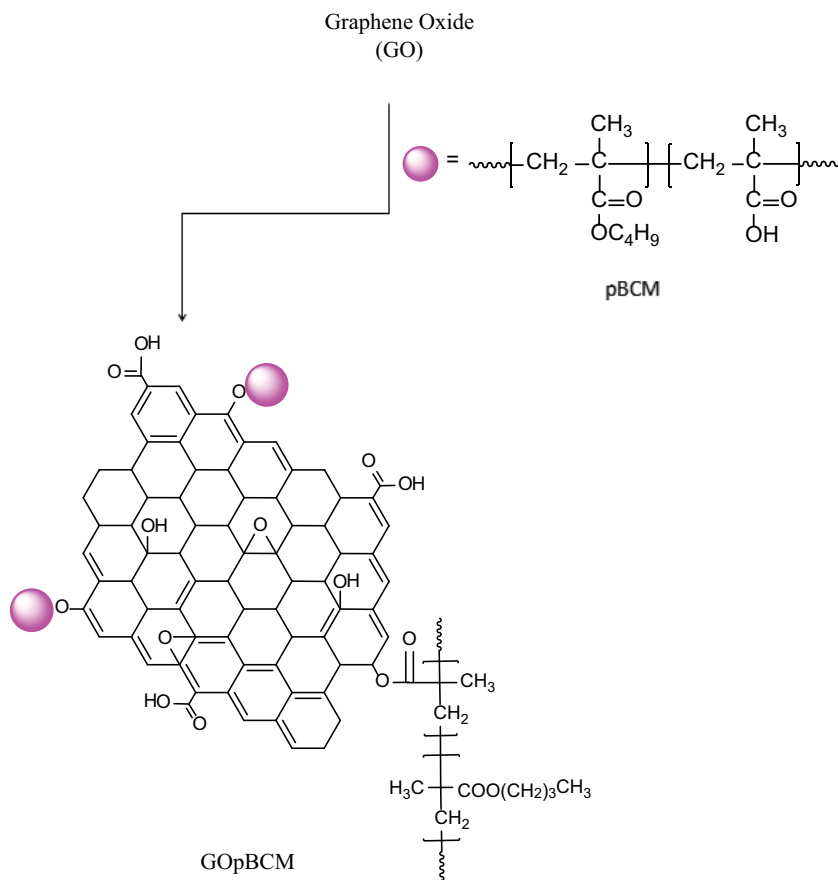
Graphene Oxide
(GO)

Fig. 2. Synthetic routes of preparing GOpBCM composite.

The mixture was stirred for additional (24 h) at room temperature. Finally, GOpBCM composite was obtained by separated, washed with DI water for over 3 times, and dried as a dark grey powder for (24 h) under vacuum [30].

2.6. Preparation of aqueous dye solution

CR dye supplied by Sigma-Aldrich Company with chemical structure shown in Fig. 3, C.I. 22120, FW = 696.7, λ_{max} = 497 nm. An anionic diazo dye is used in this study without any further treatment. A stock solution of CR dye (1,000 mg/L) was used for the adsorption experiments, and then the required concentrations were provided with the dilution by using ultra deionized water.

2.7. Adsorption experiments

Batch adsorption experiments of CR dye were carried out to evaluate the adsorption parameters and factors influencing adsorption, the number of adsorbents GO, GOCS and GOpBCM were kept at (25.0 mg) which placed into (300.0 mg/L) solution of CR dye for GO and GOpBCM, (500.0 mg/L) solution of CR for GOCS and the volume of dye was (0.1 L). The adsorption experiments were conducted on a thermostat shaker at (27°C) with a speed (200 rpm) for a specific period. After adsorption, adsorbents separated
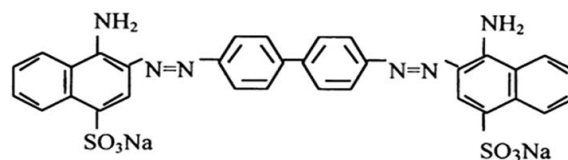

Fig. 3. Chemical structure of Congo red (CR).

from the solution by centrifugation, and the concentration of remaining CR dye was determined with a UV-T180 spectrophotometer at λ_{max} = 494 nm.

Adsorption experiments were carried out at optimum conditions applying agitation time (3, 9, 12, 15, 30, 45, and 60 min), at pH of CR dye equal 3 for GO and GOCS, 7 for GOpBCM. The amount of the dye on the adsorbents was evaluated to the following Eq. (1):

$$q_e = \frac{\left(C_0 - C_e\right)V}{m} \tag{1}$$

where C_0 and C_e (mg/L) are the initial and equilibrium concentrations of CR dye in the solution, V (L) is the volume of CR dye solution, m (g) is the mass of the used adsorbents and q_e (mg/g) is the amount of adsorbed CR dye per

gram of adsorbents GO, GOCS and GOpBCM (adsorption capacity).

To study adsorption kinetics and to calculate kinetic parameters, enthalpy ($\Delta H°$), entropy ($\Delta S°$) and free energy ($\Delta G°$), the experiments were conducted at 27°C, 40°C and 60°C, with 25.0 mg of adsorbents in 0.1 L of (300.0, 500.0, and 600.0 mg/L) solution of CR for GO, GO-g-CS, and GO-g-pBCM respectively. By varying the pH of the dye solution from 3.0 to 12.0, the maximum adsorption capacity was found at optimum pH; the adjusting of pH of the dye solution was accomplished by using 0.10 M of HCl or NaOH solution.

Desorption of the dye from the adsorbents was carried out by applying four adsorption/desorption experiments under the following criteria: using the same adsorbents, maximum adsorption of dye conducted by applying optimum agitation time, and pH-value for each adsorbent in this work. The desorption experiments were done by immersing dye-loaded adsorbent into (1.0 M) NaClO$_4$ solution, and the mixture was stirred continuously at room temperature for 60 min., then the desorbed dye was separated by centrifugation and filtration, then the concentration of dye determined spectrophotometrically as mention before [31]. The efficiency of dye desorption removal (S) was calculated by Eq. (2):

$$S = \frac{C_d \cdot V_d}{q_e \cdot W} \times 100\% \tag{2}$$

where (C_d) is the dye concentration in solution after desorption, (V_d) is the volume of the eluent.

3. Results and discussion

3.1. Characterization of the adsorbents GO, GOCS and GOpBCM

3.1.1. FTIR characterization

GO, and its composites were examined in FTIR spectroscopy as KBr discs. GO exhibits the following prominent peaks at 3,420 cm^{-1} (υ_{OH}), 1,720 cm^{-1} ($\upsilon_{C=O}$), 1,620 cm^{-1} ($\upsilon_{C=C}$), and the signals at 1,220 and 1,060 cm^{-1} were attributed to epoxy and C–O alkoxy vibrations, respectively, Fig. 4a. The FTIR spectra of GO and graphite were significantly different from the latter as it is featureless, where a high number of oxygen-containing functional groups are present on the basal planes and edges of the GO sheets [32] and the differences were generally proportionate to those that have been described in the literature [33], indicating that we successfully prepared the GO. The FTIR spectrum of GOCS composite, Fig. 4b shows a combination of characteristic peaks of chitosan and graphene oxide. So, the results implied that interactions existed between them [34], the stretching vibration bands of the C–H at 2,928 and 2,852 cm^{-1} come from (–CH$_2$–) of chitosan concluding that CS was successfully grafted on GO. The new peaks at 1,624 and 1,496 cm^{-1} (Fig. 4b) confirm the nature of the interaction between GO and CS and could be assigned to the symmetrical stretching vibration of C=O and C–N in amides (where the shift from 1,720 to 1,624 cm^{-1}) [35], and formation of amide linkages as well as the occurrence of nucleophilic substitution reactions, as proposed in the chemical interaction mechanism between GO and CS. Also, the strong and inclusive band at 3,367 cm^{-1} (O–H stretching vibration in GO carboxylic functional groups) became sharper and shifted to 3,686 cm^{-1} after the reaction with CS due to the removal of O–H in carboxylic groups forming the amides in GOCS composite [36]. Moreover, there are two characteristic absorbance bands at 1,642 and 1,577 cm^{-1}, which correspond to the (C–O) stretching vibration of (–NHCO–) and the (N–H) bends of (–NH$_2$), respectively. The absorbance peaks of the GOpBCM composite are observed at 1,625; 1,578; 1,459; 1,311; and 1,160 cm^{-1}, respectively, combining those of GO and pBCM, Fig. 4c. Furthermore, the C–O stretching vibration peak shifts from 1,720 cm^{-1} (GO) to 1,625 cm^{-1} (GOpBCM), indicating interactions between GO and pBCM chains [37,38].

3.1.2. Field emission scanning electron microscopy

The grain size and surface morphology were investigated through FESEM. According to Figs. 5a–c, GO is seen as a flat sheet with some pucker on the surface which is due to deformation of graphite upon the exfoliation processes by strong oxidizing agent KMnO$_4$ (Fig. 5a), and have well been defined and interlinked with three-dimensional graphene sheets, forming a porous network that resembles a loose sponge. On the other hand, as illustrated in (Fig. 5b), the composite appearance of GOCS is quite different compared to GO; it has some apparent folds and fluffy structures, assigned wrinkles, and curved surface. This image indicates and confirms the combination of graphene oxide and chitosan [39]. Furthermore, as seen in (Fig. 5c), the cross-section morphology of GOpBCM showed that the surface was also very compact, indicating that GO sheets were dispersed homogeneously in the polymer matrix which attributed to strong hydrogen bond interactions between graphene oxide and copolymer [40].

3.1.3. X-ray diffraction

The XRD patterns of GO, GOCS, and GOpBCM composites are shown in Fig. 6. The XRD pattern of natural graphite has a sharp diffraction peak at 2θ (26.25°), corresponding to an interlayer distance of (0.34 nm), which follows the reported value [41]. As for the GO powder sheets, Fig. 6a shows a sharp peak at 2θ position (~9.55°), which corresponds to an interlayer distance of (0.924 nm). The enlarged interlayer distance is attributed to the presence of oxygen-containing functional groups on GO sheets and suggests the successful oxidation of natural graphite using concentrated acids and KMnO$_4$ [42]. Meanwhile, after modifying GO with chitosan, Fig. 6b, many broad peaks appeared at 2θ between (~10.57°) and (~21.63°) confirming the suitable attachment of chitosan to GO surface and indicating that there is mainly a physical interaction but scarcely chemical reaction between chitosan and graphene oxide [43]. Due to the peak overlapping, no peak appeared for GO in XRD patterns of GOCS. The peak at 2θ (9.44°) of GOCS matched with that of pure GO, results from the remaining stacked GO sheets in the GOCS [34]. The peak characteristic of GO disappears in the XRD pattern of
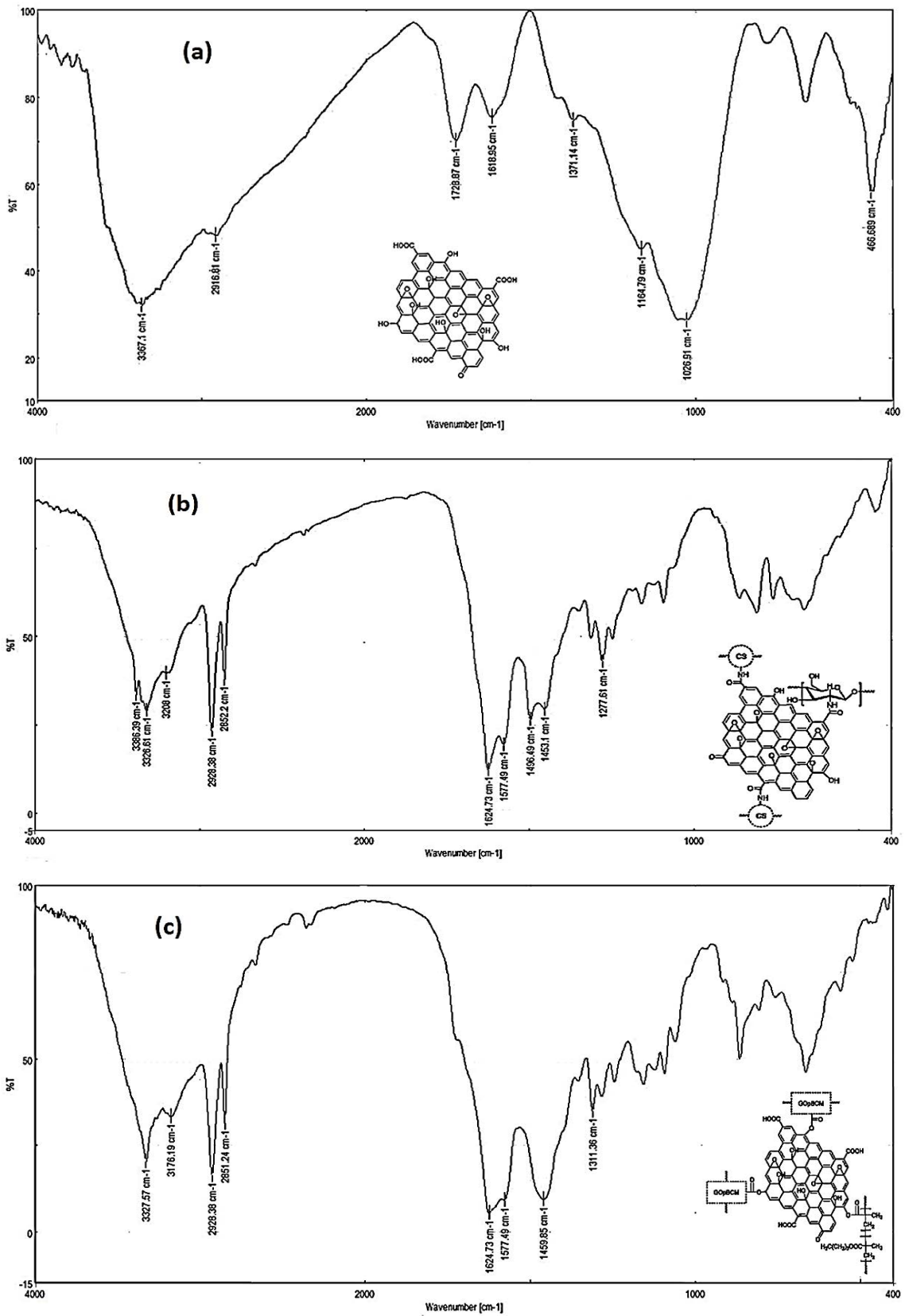
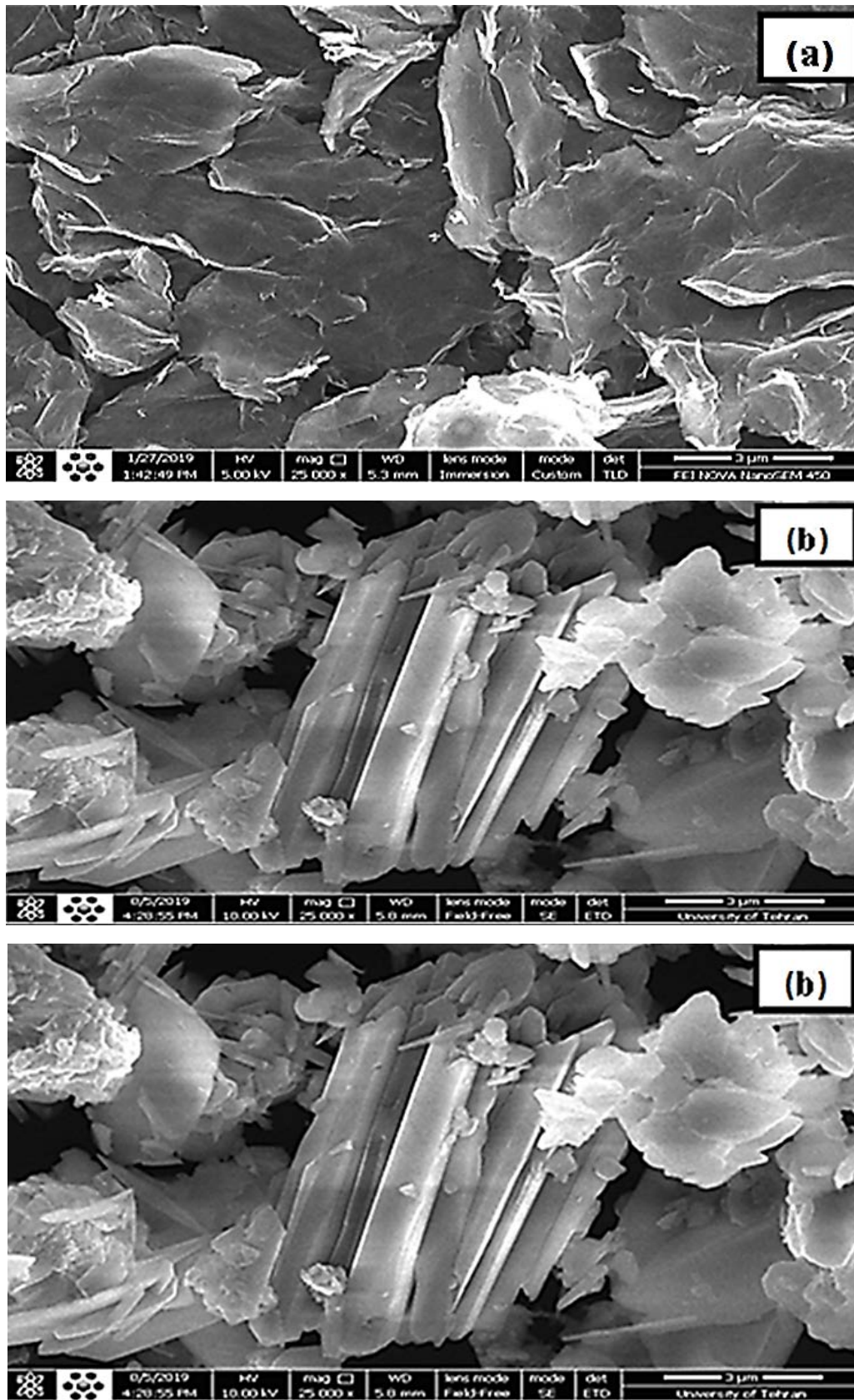Fig. 4. FTIR spectra of (a) GO, (b) GOCS, and (c) GOpBCM.

Fig. 5. FESEM images at magnification 25,000 of (a) GO, (b) GOCS, and (c) GOpBCM.
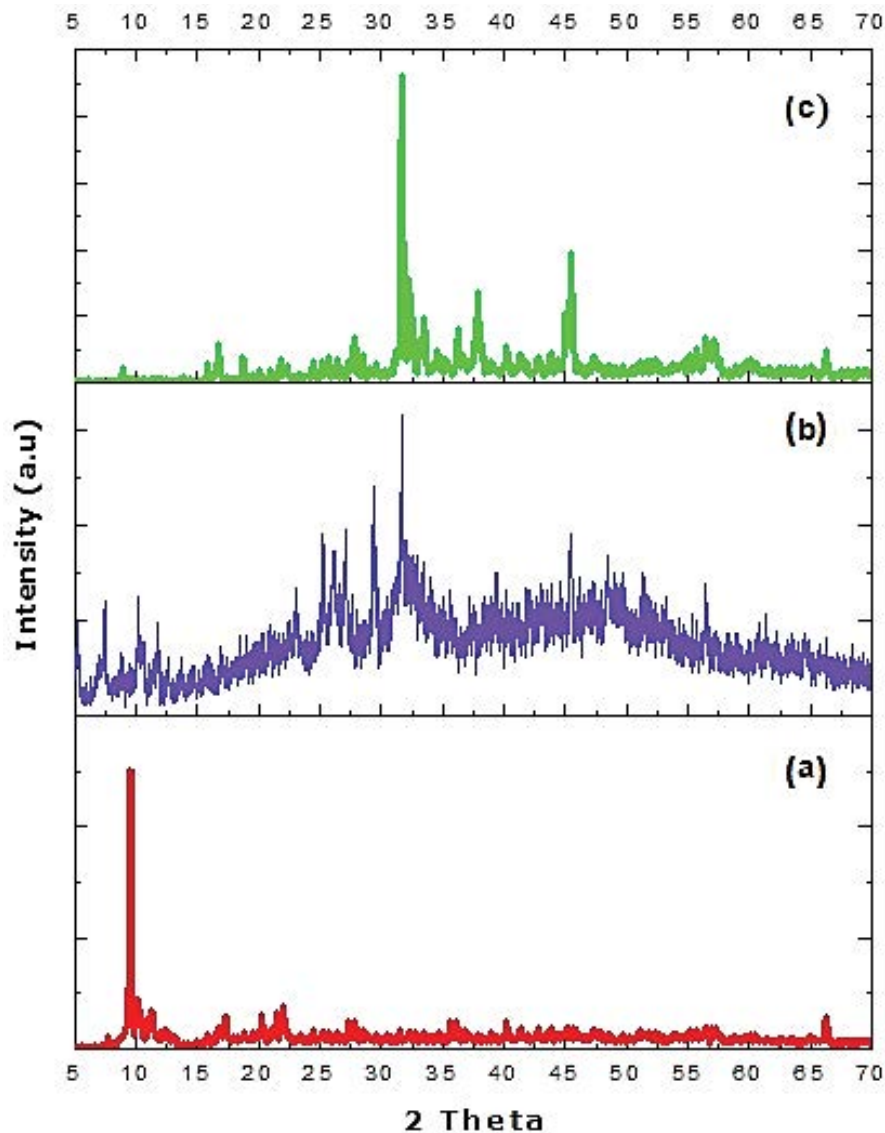
Fig. 6. XRD patterns of (a) GO, (b) GOCS, and (c) GOpBCM.

GOpBCM composite, indicating that the GO sheets are uniformly dispersed in the pBCM matrix without agglomeration [32]. On the other hand, some new characteristic peaks at 2θ 31.69°, 37.89°, and 45.47° are also observed in the XRD pattern of the GOpBCM composite, (Fig. 6c), implying real grafting had occurred.

3.1.4. Adsorption of CR dye onto GO, GOCS, and GOpBCM

The batch system was employed in adsorption experiments of CR dye onto prepared adsorbents at optimum pH, contact time, temperature, and the initial concentration (C_0).

3.2. Effect of pH

The effect of pH on the adsorption capacities (q_e) of adsorbents was studied at 300.0 and 500.0 mg/L initial concentration of CR dye for (GO and GOpBCM) and GOCS

respectively. Fig. 7 illustrates the pH influence of the adsorption capacities at different pH values ranging from 3.0 to 12.0 at 27°C. It shows a sharp decrease of CR dye adsorption was observed when as pH increased from 3.0 to 7.0, while over the range from 9.0 to 12.0, a lower adsorption capacity was found for both adsorbents GO and GOCS. However, the negative charge on adsorbents increased with increasing pH which was also reported by other studies [42]. With the increasing pH values, the adsorption of CR dye on GO and GOCS tends to decrease, which can be explained by the rising electrostatic repulsion between the anionic dye adsorbate species and negatively charged adsorbent surfaces. Also, lower adsorption at alkaline pH due to the presence of excess OH⁻ ions destabilizing anionic dye and competing with the dye anions for the adsorption sites. Low pH leads to an increase in H⁺ ion concentration in the system, the surface of adsorbents acquires a positive charge by absorbing H⁺ ions, and hence more amount of anionic dye
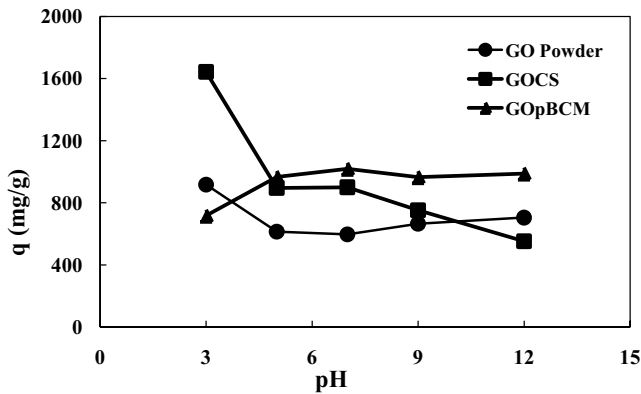
Fig. 7. Effect of pH on the adsorption of CR dye onto GO, GOCS, and GOpBCM at 27°C.

adsorption takes place. Similar behavior was observed for CR dye adsorption on agricultural stable waste-based activated carbon [43]. Fig. 7 reveals that the best pH value found is 7.0 for the better adsorption of CR by GOpBCM. Thus, in the further followed experiments, the pH was kept at pH 7.0. Similar results have been reported for the removal of CR dye by sorption onto aniline propyl silica aerogel [44].

3.3. Effects of agitation time and temperature on the adsorption

The duration time before the adsorption process reaches equilibrium called agitation time [31], Fig. 8 shows the plots for the effect of agitation time on the adsorption of CR dye at pH 3.0 onto adsorbents GO, GOCS and at pH 7.0 onto GOpBCM composites at different temperatures. It can be seen that the adsorption of CR has rapidly increased from (1–60 min), and then the equilibrium was attained within (60–90 min) for adsorbents GO and GOpBCM respectively, (Figs. 8a and c); also, the adsorption capacity for both increased as temperature rising from 27°C to 60°C.

The adsorption equilibrium time was 60 min for GO and GOpBCM. Since the adsorption was endothermic. While Fig. 8b shows the rapid increase for adsorbent GOCS from (1–45 min), then equilibrium was attained within (45–75 min), and the adsorption capacity for this adsorbent decreased as temperature rising from 27°C to 60°C where the adsorption equilibrium time was 45 min and the adsorption were exothermic. This tendency for the adsorption capacities of these adsorbents is expected. Thus, the optimum agitation times for all further experiments were chosen as 60 min for adsorption of CR dye by adsorbents GO, GOpBCM, and 45 min for adsorption of CR dye onto GOCS.

3.4. Adsorption isotherms

The adsorption isotherm shows the distribution of molecules between solid and liquid phases at equilibrium state. The analysis of isotherm data by fitting the data to different isotherm models is an essential step in finding the most suitable model that can be used to describe the adsorption process [45]. There are several isotherm models to describe the isotherm data. In the present study, Langmuir, Freundlich, and Temkin isotherm models are employed to
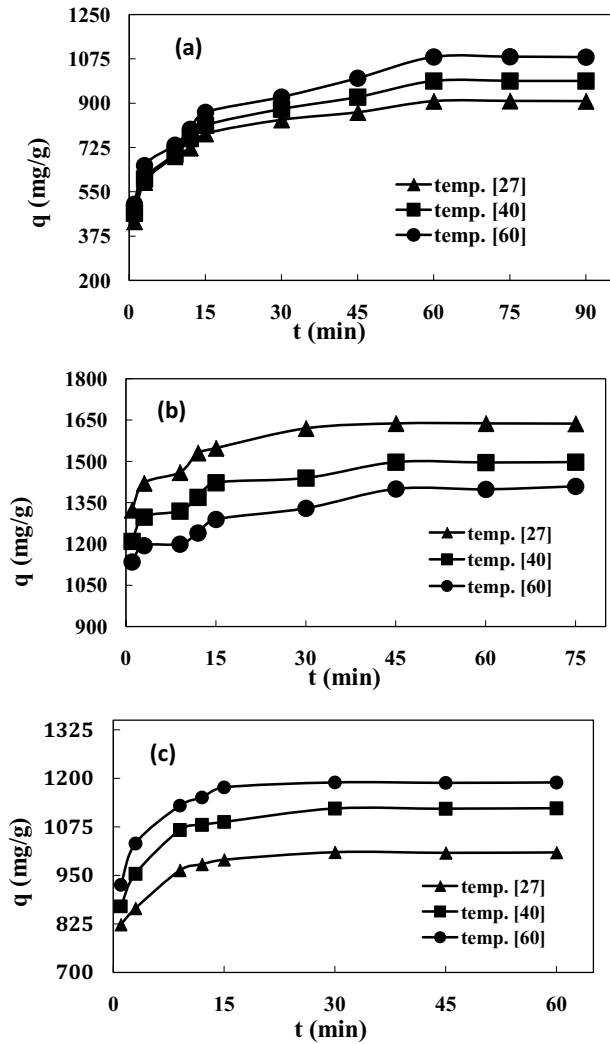

Fig. 8. Agitation time effects for the adsorption of CR dye onto (a) GO, (b) GOCS, and (c) GOpBCM at 27°C, 40°C, and 60°C.

analyze the experimental results. The Langmuir isotherm [46] depends upon the maximum adsorption that coincides with the saturated monolayer of liquid (adsorbate) molecules on the solid (adsorbent) surface. The linearized form of the Langmuir model is given as follows.

$$\frac{C_e}{q_e} = \frac{1}{q_{max} \cdot K_L} + \frac{C_e}{q_{max}} \tag{3}$$

Langmuir equation is valid for monolayer adsorption of the adsorbate onto the surface of the adsorbent and assumes there are restricted and homogenous adsorption sites [47]. Royer et al. [48] noted that the essential characteristics of a Langmuir isotherm can be expressed in terms of dimensionless constant separation factor or equilibrium parameter R_L, which is defined by:

$$R_L = \frac{1}{1 + (K_L \cdot C_e)} \tag{4}$$

where R_L is indicative of the isotherm shape and predicts whether a sorption system to be either favourable ($0 < R_L < 1$), unfavourable ($R_L > 1$) or irreversible ($R_L = 0$) [49,50]. Fig. 9a shows the plots of the Langmuir adsorption isotherms of CR dye adsorbed onto GO, GOCS and GOpBCM respectively, Table 1 displays q_{max}, K_L, R_L and the correlation coefficient (R^2) results for the Langmuir isotherms.

In the present study, the calculated R_L values were found to be equal (0.09639, 0.04251, and 0.04724) at initial concentrations of CR dye 300.0, 500.0, and 300.0 mg/L for GO, GOCS, and GOpBCM respectively. These calculated results proved that all adsorbents are favorable for adsorbing dye from solution under the applied optimum conditions.

Freundlich isotherm [51] is based on a heterogeneous exponentially decaying distribution, which fits well with the tail portion of the heterogeneous distribution of adsorbent. The general Freundlich isotherm empirical equation is given by:
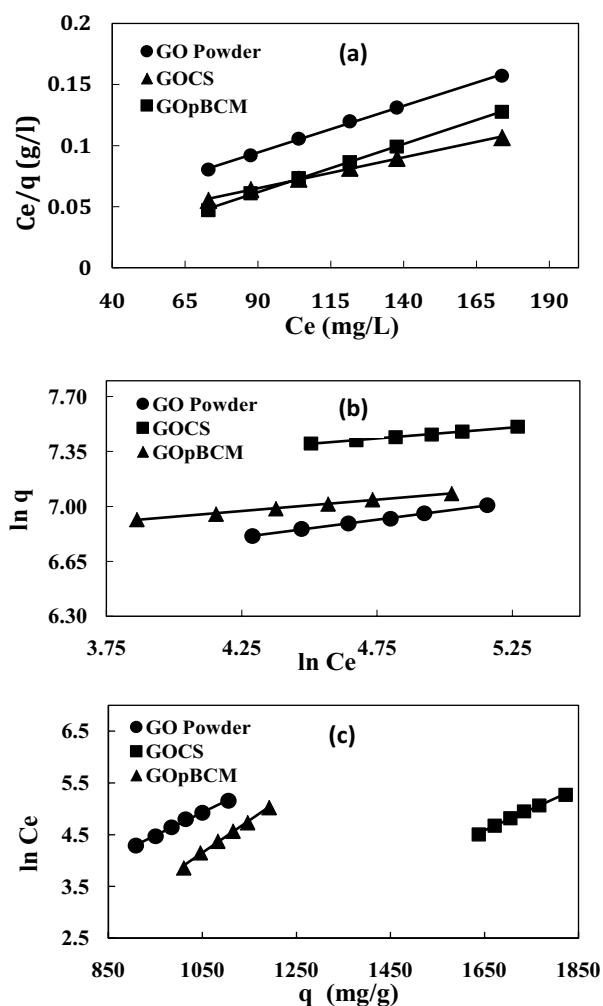
$$\ln q_e = \ln K_F + \frac{1}{n}\ln C_e \tag{5}$$

Fig. 9. (a) Langmuir, (b) Freundlich, and (c) Temkin adsorption isotherm of CR dye onto GO, GOCS, and GOpBCM at 27°C.

where K_F (L/mg) is a constant for the adsorption or distribution coefficient and represents the amount of dye adsorbed onto adsorbents at equilibrium concentration, Fig. 9b exhibits the plots of Freundlich adsorption isotherms of CR adsorbed onto GO, GOCS, and GOpBCM and Table 1 display K_F, n and the correlation coefficient R^2 which determined from the linear plot of $\ln q_e$ vs. $\ln C_e$. The value of n varies with the heterogeneity of the adsorbent and the favorable adsorption process should be higher than unity and less than 10 [52]. All n values obtained from the Freundlich model are greater than 1 for all types of adsorbents used; indicating that adsorption of CR was favorable for the prepared composites.

The Temkin isotherm [53] assumes that the heat of adsorption of all the molecules decreases linearly with the coverage of the molecules due to the adsorbate–adsorbate repulsion and the adsorption of adsorbate is uniformly distributed and that the fall in the heat of adsorption is more linear rather than logarithmic [54]. It is expressed as:

$$q_e = B_T \ln A_T + B_T \ln C_e \tag{6}$$

where $B_T = RT/b_T$, T (K) is absolute temperature, and R is the gas constant (8.31 J/mol K). The constant b_T is related to the heat of adsorption, and A_T is equilibrium binding constant coinciding to the maximum binding energy. The plot of q_e vs. $\ln C_e$ for the Temkin model is shown in Fig. 9c. The values of B_T and A_T are determined from the slope and intercept and are given in Table 1. The values of the correlation coefficient (R^2) were 0.9967, 0.9951, and 0.9958 for GO, GOCS, and GOpBCM, respectively, which are lower than the Langmuir model indicating the adsorption data was not fitted to the Temkin model.

Table 1 shows the linearity of the Langmuir isotherm equation was more fitting with comparing that isotherm equation of Freundlich and Temkin, where inspire of the complexity of adsorption processes, but it could say there was a tendency for chemical adsorption to exist between functional groups of adsorbents GO, GOCS and GOpBCM and CR dye. The values of ($1/n$) obtained from the slope of Freundlich isotherm plots were (<1), indicated normal Langmuir isotherm behaviors of dye adsorption onto adsorbents [47].

3.5. Adsorption kinetics

Three kinetic models were tested to interpret the mechanism of adsorption of CR dye onto GO, GOCS, and GOpBCM. The first model was pseudo-first-order, the mathematical expression of this model given by Eq. (7):

$$\frac{1}{q_t} = \frac{k_1}{q_1 \cdot t} + \frac{1}{q_1} \tag{7}$$

where q_t and q_1 (mg/g) are the amounts of dye adsorbed at time t, and equilibrium respectively, and k_1 (min^{-1}) is the pseudo-first-order rate constant for adsorption. Plotting of $1/q_t$ vs. $1/t$ results in the rate constants k_1, and correlation coefficients R^2. Fig. 10 illustrates the pseudo-first-order equations

Table 1
Langmuir, Freundlich and Temkin isotherm parameters for adsorption of CR dye onto adsorbents at 27°C

Adsorbent	Langmuir				Freundlich			Temkin			
	q_{max}	K_L	R_L	R^2	K_F	n	R^2	B_T	A_T	R^2	
GO	1,250	0.031	0.097	0.9987	348.278	4.484	0.9982	566,864	6E+25	0.9967	
GOCS	2,000	0.045	0.043	0.9994	877.608	7.246	0.9981	608,341	4E+234	0.9951	
GOpBCM	1,250	0.067	0.047	0.9992	573.237	6.849	0.9975	402,290	4E+167	0.9958	

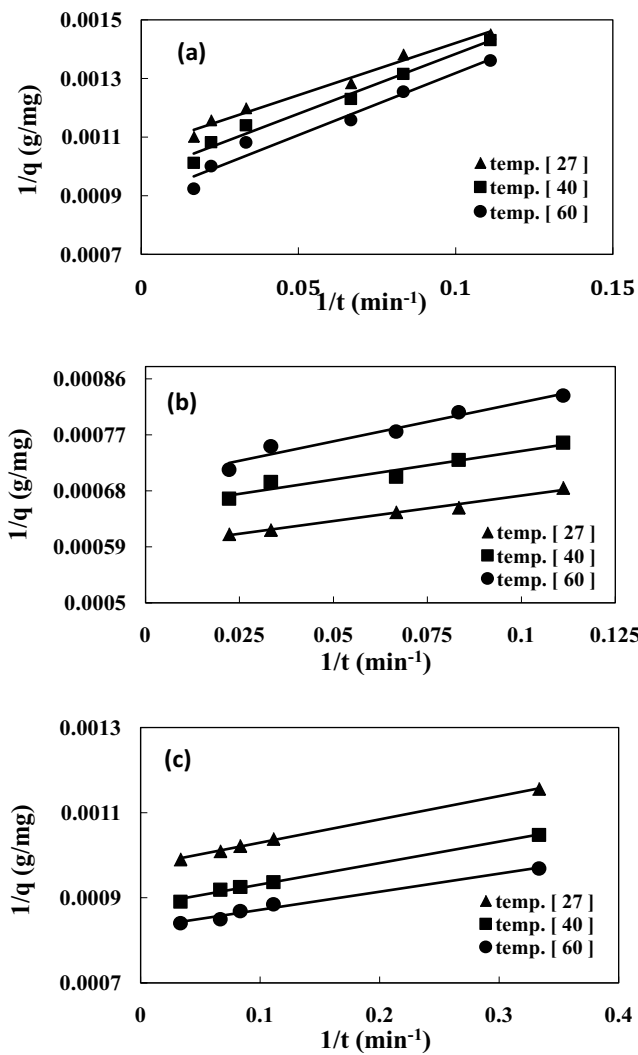K_L: (L/mg); q_{max}: (mg/g); B_T: (J/mol); A_T: (L/mg)

Fig. 10. Pseudo-first-order plots for the adsorption of CR dye onto (a) GO, (b) GOCS, and (c) GOpBCM at 27°C, 40°C, and 60°C.

for CR dye at different temperatures, the k_1 and q_1 values are listed in Table 2.

The second kinetic model was pseudo-second-order, which can be represented by Eq. (8):

$$\frac{t}{q_t} = \frac{1}{K_2 \cdot q_2^2} + \frac{1}{q_2}$$ (8)

where q_2 (mg/g) are the maximum adsorption capacity for the pseudo-second-order adsorption, k_2 (g mg^{-1} min^{-1}) is the equilibrium rate constant for the pseudo-second-order adsorption. Values of q_2 and k_2 were calculated from the plot of (t/q_t) against (t) from the slope and intercept, respectively Fig. 11. The kinetic data for the adsorption of CR dye onto GO, GOCS, and GOpBCM under various temperatures were calculated from related plots and are summarized in Table 2.

Intra-particle diffusion was the last model tested in this study; equation of intra-particle diffusion model given by:

$$q_t = \left(K_p \cdot t^{\frac{1}{2}} \right) + C$$ (9)

where C is the intercept, and K_p (mg g^{-1} min$^{-1/2}$) is the intra-particle diffusion rate constant that equal to the slope of plotting between q_t vs. $t^{-1/2}$. Fig. 12 displays the intra-particle diffusion models for CR dye at different temperatures; Table 2 gives K_p and C values.

3.6. Adsorption thermodynamics

The thermodynamic parameters can be determined from the thermodynamic equilibrium constant, K_L (or the thermodynamic distribution coefficient), whereas K_L equal to:

$$K_L = \frac{C_a}{C_e}$$ (10)

where C_a and C_e are the equilibrium concentrations of CR dye on the adsorbents GO, GOCS and GOpBCM (mg/g) and in the solution (mg/L), respectively.

The standard enthalpy change ($\Delta H°$ in kJ/mol), and standard entropy change) ($\Delta S°$ in J mol^{-1} K^{-1}) were calculated using the following equation:

$$\ln K_L = \frac{\Delta S°}{R} = \frac{\Delta H°}{RT}$$ (11)

where R is the universal gas constant (8.314 J/mol K), and T is the absolute temperature, plotting of ($\ln K_L$) vs. ($1/T$) leading to calculate $\Delta H°$ from slope and $\Delta S°$ from an intercept, Fig. 13. The standard Gibbs free energy ($\Delta G°$ in kJ/mol) could be calculated at different temperatures from the following equation:

$$\Delta G° = \Delta H° - T\Delta S°$$ (12)

Table 2
Kinetic parameters for adsorption of CR dye onto adsorbents at constant pH and different temperatures

| Adsorbent	GO			GOCS			GOpBCM		
$T/°C$	27°C	40°C	60°C	27°C	40°C	60°C	27°C	40°C	60°C
Pseudo-first-order									
q_1 (mg/g)	909	1,000	1,111	16,666	1,428	1,428	1,000	1,111	2,500
k_1 (1/min)	3.27	4.10	4.66	1.33	1.28	1.85	0.50	0.55	2.00
R_1^2	0.980	0.980	0.966	0.986	0.939	0.960	0.998	0.994	0.984
Pseudo-second-order									
q_2 (mg/g)	1,000	1,000	1,111	1,666	1,428	1,428	1,000	1,111	1,250
$k_2 \times 10^{-8}$ (g/mg min)	2.60	2.20	1.60	0.60	0.40	3.00	1.66	1.35	1.28
R_2^2	0.999	0.996	0.995	0.999	0.999	0.999	1.000	0.999	0.999
Intraparticle diffusion equation									
K_p	42.93	54.66	66.19	43.78	41.00	49.16	37.108	42.622	41.401
C	583	568	566	1,326	1,225	1,070	831	913	991
R_p^2	0.948	0.957	0.966	0.886	0.868	0.949	0.800	0.827	0.816
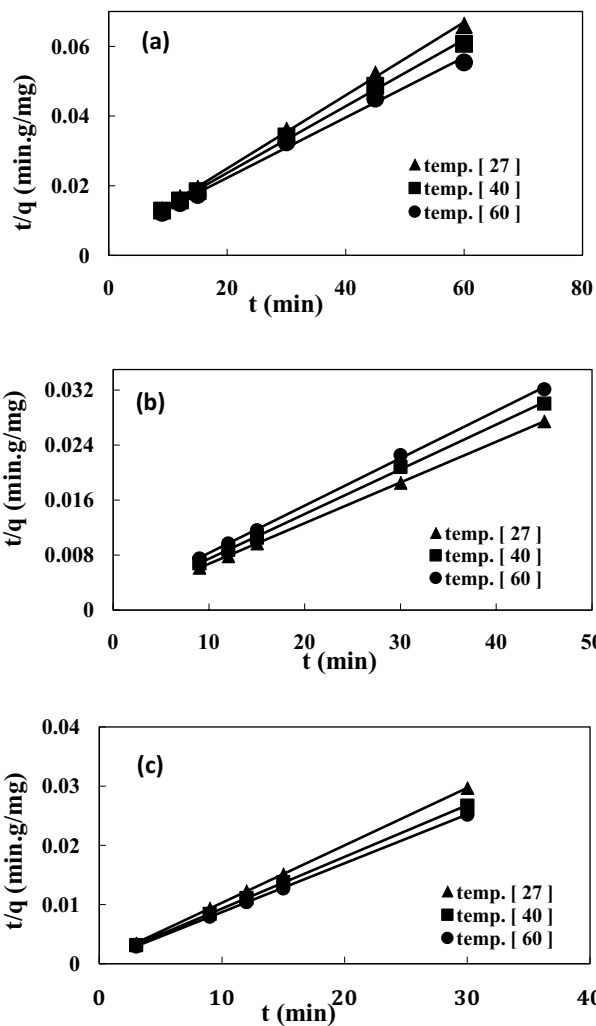
Fig. 11. Pseudo-second-order plots for the adsorption of CR dye onto (a) GO, (b) GOCS, and (c) GOpBCM at 27°C, 40°C, and 60°C.
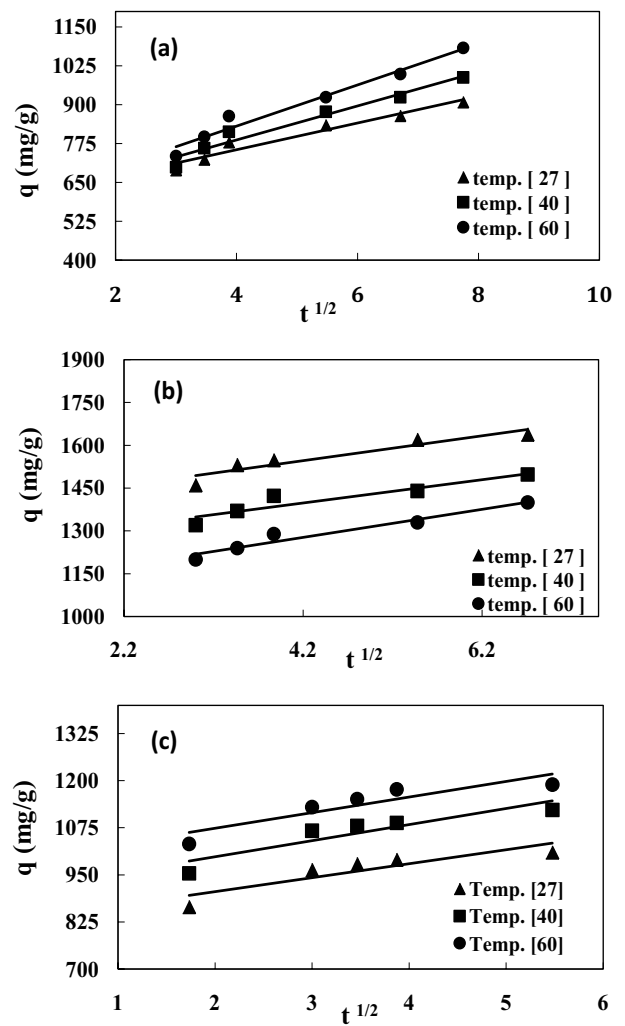

Fig. 12. Intra-particle diffusion plots for the adsorption of CR dye onto (a) GO, (b) GOCS, and (c) GOpBCM at 27°C, 40°C, and 60°C.

The activation energy (E_a in kJ/mol) which may be defined as the minimum amount of energy required to adsorption process proceeds, and it was calculated from the Arrhenius equation:

$$\ln K = \ln A - \frac{E_a}{RT} \tag{13}$$

where K (g mg^{-1} min^{-1}) is the rate constant of the pseudo-second-order kinetic model in an adsorption system of the CR dye for all adsorbents, because the adsorption analyses based on the constant obtained from the linearized plots (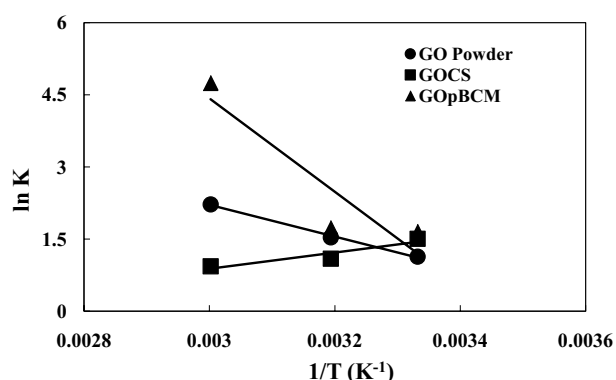R^2), A is the Arrhenius factor, when ($\ln K$) is plotted against ($1/T$), where a straight line is obtained (with a slope of $-E_a/R$) as shown in Fig. 14, The values of $\Delta H°$, $\Delta S°$, $\Delta G°$, and E_a for the adsorption of CR dye onto adsorbents GO, GOCS, and GOpBCM composites are given in Table 3.

The calculated thermodynamic parameters show positive values of enthalpy changes ($\Delta H°$) for GO and GOpBCM composite, indicating that the adsorption processes were endothermic, also the positive value of adsorption entropy ($\Delta S°$) suggests an increase in the randomness at the (adsorbents/solution) interface and affinity of the mentioned adsorbents towards dye. While GOCS composite shows the negative value of both enthalpy and adsorption entropy ($\Delta H°$ and $\Delta S°$), indicating that the process is exothermic and the mobility of the adsorbate (CR) onto adsorbent GOCS becomes more limited as compared with that of this in the

Fig. 13. Plots of $\ln K$ vs. $1/T$ for estimation of thermodynamic parameters for the adsorption of CR dye onto GO, GOCS, and GOpBCM.
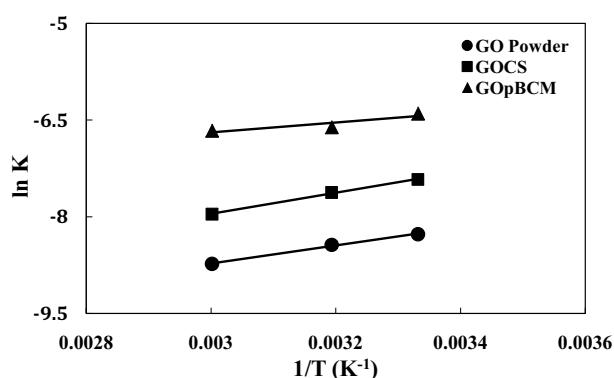

Fig. 14. Plots of $\ln K$ vs. $1/T$ for estimation of activation energy for the adsorption of CR dye onto GO, GOCS, and GOpBCM.

Table 3
Thermodynamic parameters for adsorption of CR dye onto adsorbents at different temperatures

Adsorbent	T (K)	$\Delta H°$ (kJ/mol)	$\Delta S°$ (J/K mol)	$-\Delta G°$ (kJ/mol)	E_a (kJ/mol)
GO	300.15			2.78	
	313.15	27.46	100.76	4.09	11.642
	333.15			6.11	
GOCS	300.15			3.60	
	313.15	−13.99	-34.622	3.15	13.641
	333.15			2.45	
GOpBCM	300.15			3.00	
	313.15	80.74	279.00	6.63	6.380
	333.15			12.21	

Table 4
Adsorption/desorption for CR dye onto adsorbents

Cycle number	GO		GOCS		GOpBCM	
	q_e	%S	q_e	%S	q_e	%S
1	1,000	84.41	1,666	94.87	1,000	90.03
2	673.14	80.05	1,468.54	91.55	829.65	86.87
3	588.92	76.79	1,377.11	88.91	789.40	84.77

q_e: (mg/g); %S: desorption system

solution [47]. The obtained values of the free energy changes $\Delta G°$ at different temperatures were less than zero for all adsorbents in this work, denoting the behavior of adsorption processes is spontaneous and feasible [55]. Low activation energy E_a values (<40 kJ/mol) are characteristics of the physisorption mechanism and diffusion-controlled process. Therefore, these results indicate that the adsorption processes of CR dye onto GO, GOCS, and GOpBCM composites are diffusion-controlled and physical.

3.7. Desorption study

Desorption studies are an important to elucidate the reusability of an adsorbent and to understand the nature of adsorption system and evaluate the ability of recycling and Table 4 show the desorption percentages of at the three-cycle were (76.79%, 88.91%, and 84.77%) for CR adsorbed GO, GOCS and GOpBCM respectively, that is meant that these adsorbents could be used several times while retaining its good adsorption capacity.

4. Conclusions

The present work suggests that GOCS and GOpBCM composites can be used as an adsorbent for the removal of CR dye from aqueous solutions. GOCS and GOpBCM composites were synthesized by grafting the prepared GO and they have been characterized by an FTIR, FESEM, and X-rays confirming that real grafting has occurred. The equilibrium data were described by the Langmuir, Freundlich and Temkin, and the results fitted well with the Langmuir model implying that the adsorption process is favorable for a monolayer chemisorption coverage. The maximum adsorption values (q_{max}) of CR dye where 1,666 mg/g for GOCS composite and 1,000 mg/g for GO and GOpBCM composites. Depending on the value of the correlation coefficient R^2, the pseudo-second-order kinetic model accurately described the adsorption kinetics of CR dye onto the three adsorbents used. It was found that the adsorption capacity increased with temperature increasing for GO and GOpBCM, and decreased for GOCS. The negative free energy ($\Delta G°$) demonstrated that the adsorption of CR onto GO, GOCS, and GOpBCM adsorbents is spontaneous. However, the positive enthalpy ($\Delta H°$) for GO and GOpBCM composites indicated the endothermic nature of their adsorption, while the negative $\Delta H°$ value for GOCS indicated the exothermic nature of the adsorption process at the examined temperatures range. The positive entropy ($\Delta S°$) reflects increased randomness at the solid-solution interface during the CR adsorption onto GO and GOpBCM composite. On the other hand, the negative value of $\Delta S°$ obtained from the adsorption of CR onto GOCS referred to the mobility limitation of the dye accompanied by the decrease randomness of the solid/solution interfaces during the adsorption of CR dye. The impact of the obtained results gave the study potential importance towards different applications of the prepared composites concerning better industrial wastewater treatment.

References

[1] Z. Harrache, M. Abbas, T. Aksil, M. Trari, Thermodynamic and kinetics studies on adsorption of Indigo Carmine from aqueous solution by activated carbon, Microchem. J., 144 (2019) 180–189.

[2] U. Mir Khan, Z. Selamoglu, Treatment of biosorption and ozonation on elimination of the day pollution in treated water, Surv. Fish. Sci., 6 (2020) 21–25.

[3] S. Madan, R. Shaw, S. Tiwari, S.K. Tiwari, Adsorption dynamics of Congo red dye removal using ZnO functionalized high silica zeolitic particles, Appl. Surf. Sci., 487 (2019) 907–917.

[4] D. Yuan, D.Y. Fu, C.X. Wang, Selective removal of Congo red from wastewater using molecularly imprinted polymer, Sep. Sci. Technol., (2020) 1–9, https://doi.org/10.1080/01496395.2020.1715435.

[5] J.N. Wekoye, W.C. Wanyonyi, P.T. Wangila, M.K. Tonui, Kinetic and equilibrium studies of Congo red dye adsorption on cabbage waste powder, Environ. Chem. Ecotoxicol., 2 (2020) 24–31.

[6] R.J. Li, X.-a. Ning, J. Sun, Y.J. Wang, J.Y. Liang, M.Q. Lin, Y.P. Zhang, Decolorization and biodegradation of the Congo red by *Acinetobacter baumannii YNWH 226* and its polymer production's flocculation and dewatering potential, Bioresour. Technol., 194 (2015) 233–239.

[7] L. Singh, P. Rekha, S. Chand, Cu-impregnated zeolite Y as highly active and stable heterogeneous Fenton-like catalyst for degradation of Congo red dye, Sep. Purif. Technol., 170 (2016) 321–336.

[8] A.M.S. Solano, S. Garcia-Segura, C.A. Martínez-Huitle, E. Brillas, Degradation of acidic aqueous solutions of the diazo dye Congo Red by photo-assisted electrochemical processes based on Fenton's reaction chemistry, Appl. Catal., B, 168–169 (2015) 559–571.

[9] M. Laabd, H.A. Ahsaine, A. El Jaouhari, B. Bakiz, M. Bazzaoui, M. Ezahri, A. Albourine, A. Benlhachemi, Congo red removal by PANi/Bi_2WO_6 nanocomposites: kinetic, equilibrium and thermodynamic studies, J. Environ. Chem. Eng., 4 (2016) 3096–3105.

[10] M. Thomas, G.A. Naikoo, M. Ud Din Sheikh, M. Bano, F. Khan, Effective photocatalytic degradation of Congo red dye using alginate/carboxymethyl cellulose/TiO_2 nanocomposite hydrogel under direct sunlight irradiation, J. Photochem. Photobiol., A, 327 (2016) 33–43.

[11] H.-Y. Zhu, R. Jiang, Y.-Q. Fu, R.-R. Li, J. Yao, S.-T. Jiang, Novel multifunctional $NiFe_2O_4$/ZnO hybrids for dye removal by adsorption, photocatalysis and magnetic separation, Appl. Surf. Sci., 369 (2016) 1–10.

[12] Y.J. Yao, S.D. Miao, S.M. Yu, L.P. Ma, H.Q. Sun, S.B. Wang, Fabrication of Fe_3O_4/SiO_2 core/shell nanoparticles attached to graphene oxide and its use as an adsorbent, J. Colloid Interface Sci., 379 (2012) 20–26.

[13] X.Y. Gu, Y. Ning, Y. Yang, C.Y. Wang, One-step synthesis of porous graphene-based hydrogels containing oil droplets for drug delivery, RSC Adv., 4 (2014) 3211–3218.

[14] R. Justin, B.Q. Chen, Strong and conductive chitosan–reduced graphene oxide nanocomposites for transdermal drug delivery, J. Mater. Chem. B, 2 (2014) 3759–3770.

[15] S.Z.N. Ahmad, W.N.W. Salleh, A.F. Ismail, N. Yusof, M.Z.M. Yusop, F. Aziz, Adsorptive removal of heavy metal ions using graphene-based nanomaterials: toxicity, roles of functional groups and mechanisms, Chemosphere, 248 (2020) 126008.

[16] L.Y. Kan, Z. Xu, C. Gao, General avenue to individually dispersed graphene oxide-based two-dimensional molecular brushes by free radical polymerization, Macromolecules, 44 (2010) 444–452.

[17] Y.F. Yang, Y.L. Xie, L.C. Pang, M. Li, X.H. Song, J.G. Wen, H.Y. Zhao, Preparation of reduced graphene oxide/poly (acrylamide) nanocomposite and its adsorption of Pb(II) and methylene blue, Langmuir, 29 (2013) 10727–10736.

[18] J.K. Liu, H.Q. Cao, J.P. Xiong, Z.Y. Cheng, Ferromagnetic hematite@graphene nanocomposites for removal of rhodamine B dye molecules from water, CrystEngComm, 14 (2012) 5140–5144.

[19] V. Chandra, J.S. Park, Y. Chun, J.W. Lee, I.-C. Hwang, K.S. Kim, Water-dispersible magnetite-reduced graphene oxide composites for arsenic removal, ACS Nano, 4 (2010) 3979–3986.

[20] L.L. Li, L.L. Fan, H.M. Duan, X.J. Wang, C.N. Luo, Magnetically separable functionalized graphene oxide decorated with

magnetic cyclodextrin as an excellent adsorbent for dye removal, RSC Adv., 4 (2014) 37114–37121.

[21] J.W. Zhang, M.S. Azam, C. Shi, J. Huang, B. Yan, Q.X. Liu, H.B. Zeng, Poly(acrylic acid) functionalized magnetic graphene oxide nanocomposite for removal of methylene blue, RSC Adv., 5 (2015) 32272–32282.

[22] V. Chandra, K.S. Kim, Highly selective adsorption of Hg^{2+} by a polypyrrole–reduced graphene oxide composite, Chem. Commun., 47 (2011) 3942–3944.

[23] R.J. Li, L.F. Liu, F.L. Yang, Preparation of polyaniline/reduced graphene oxide nanocomposite and its application in adsorption of aqueous Hg(II), Chem. Eng. J., 229 (2013) 460–468.

[24] L. Yang, Z.C. Li, G.D. Nie, Z. Zhang, X.F. Lu, C. Wang, Fabrication of poly(o-phenylenediamine)/reduced graphene oxide composite nanosheets via microwave heating and their effective adsorption of lead ions, Appl. Surf. Sci., 307 (2014) 601–607.

[25] A.O. da Silva, R.P. Weber, S.N. Monteiro, A.M. Lima, G.S. Faria, W.O. da Silva, S. de Sant'Ana Oliveira, K.G. de Castro Monsores, W.A. Pinheiro, Effect of graphene oxide coating on the ballistic performance of aramid fabric, J. Mater. Res. Technol., 9 (2020) 2267–2278.

[26] R.M. Islamova, O.I. Golovochesova, Y.B. Monakov, I.A. Utepova, A.A. Musikhina, O.N. Chupakhin, Effect of heterocyclic derivatives of ferrocene on free-radical polymerization of methyl methacrylate and styrene, Polym. Sci. Ser. B Polym. Chem., 52 (2010) 637–647.

[27] L.P. Krul', L.B. Yakimtsova, E.L. Egorova, Y.I. Matusevich, K.A. Selevich, A.L. Kurtikova, Preparation and thermal degradation of methyl methacrylate-methacrylic acid copolymers, Russ. J. Appl. Chem., 82 (2009) 1636–1643.

[28] L.L. Li, C. Luo, X.J. Li, H.M. Duan, X.J. Wang, Preparation of magnetic ionic liquid/chitosan/graphene oxide composite and application for water treatment, Int. J. Biol. Macromol., 66 (2014) 172–178.

[29] D. Depan, B. Girase, J.S. Shah, R.D.K. Misra, Structure–process–property relationship of the polar graphene oxide-mediated cellular response and stimulated growth of osteoblasts on hybrid chitosan network structure nanocomposite scaffolds, Acta Biomater., 7 (2011) 3432–3445.

[30] J.S. Liu, G.N. Liu, W.X. Liu, Preparation of water-soluble β-cyclodextrin/poly(acrylic acid)/graphene oxide nanocomposites as new adsorbents to remove cationic dyes from aqueous solutions, Chem. Eng. J., 257 (2014) 299–308.

[31] S. Mohebali, D. Bastani, H. Shayesteh, Equilibrium, kinetic and thermodynamic studies of a low-cost biosorbent for the removal of Congo red dye: acid and CTAB-acid modified celery (*Apium graveolens*), J. Mol. Struct., 1176 (2019) 181–193.

[32] M. Zhong, Y.-T. Liu, X.-M. Xie, Self-healable, super tough graphene oxide–poly(acrylic acid) nanocomposite hydrogels facilitated by dual cross-linking effects through dynamic ionic interactions, J. Mater. Chem. B, 3 (2015) 4001–4008.

[33] J.B. Ma, P. Cai, W. Qi, D.H. Kong, H. Wang, The layer-by-layer assembly of polyelectrolyte functionalized graphene sheets: a potential tool for biosensing, Colloids Surf., A, 426 (2013) 6–11.

[34] W.M.A. El Rouby, A.A. Farghali, M.A. Sadek, W.F. Khalil, Fast removal of Sr(II) from water by graphene oxide and chitosan modified graphene oxide, J. Inorg. Organomet. Polym. Mater., 28 (2018) 2336–2349.

[35] M.S.H. Akash, K. Rehman, Introduction to Spectrophotometric Techniques, In: Essentials of Pharmaceutical Analysis, Springer, Singapore, 2020, pp. 19–27.

[36] M. Ghorbani, A. Shams, O. Seyedin, N.A. Lahoori, Magnetic ethylene diamine-functionalized graphene oxide as novel sorbent for removal of lead and cadmium ions from wastewater samples, Environ. Sci. Pollut. Res., 25 (2018) 5655–5667.

[37] S.J. Park, K.-S. Lee, G. Bozoklu, W.W. Cai, S.T. Nguyen, R.S. Ruoff, Graphene oxide papers modified by divalent ions–enhancing mechanical properties *via* chemical cross-linking, ACS Nano, 2 (2008) 572–578.

[38] H.-P. Cong, P. Wang, S.-H. Yu, Highly elastic and superstretchable graphene oxide/polyacrylamide hydrogels, Small, 10 (2014) 448–453.

[39] S. Kumar, J.S. Koh, Physiochemical and optical properties of chitosan based graphene oxide bionanocomposite, Int. J. Biol. Macromol., 70 (2014) 559–564.

[40] Y.W. Huang, M. Zeng, J. Ren, J. Wang, L.R. Fan, Q.Y. Xu, Preparation and swelling properties of graphene oxide/poly(acrylic acid-co-acrylamide) super-absorbent hydrogel nanocomposites, Colloids Surf., A, 401 (2012) 97–106.

[41] G.J. Liu, L. Wang, B. Wang, T.T. Gao, D.L. Wang, A reduced graphene oxide modified metallic cobalt composite with superior electrochemical performance for supercapacitors, RSC Adv., 5 (2015) 63553–63560.

[42] T.N. Blanton, D. Majumdar, Characterization of X-ray irradiated graphene oxide coatings using X-ray diffraction, X-ray photoelectron spectroscopy, and atomic force microscopy, Powder Diffr., 28 (2013) 68–71.

[43] D.L. Han, L.F. Yan, W.F. Chen, W. Li, Preparation of chitosan/graphene oxide composite film with enhanced mechanical strength in the wet state, Carbohydr. Polym., 83 (2011) 653–658.

[44] Y.H. Cai, B. Tang, L.Y. Bin, S.S. Huang, P. Li, F.L. Fu, Constructing a multi-layer adsorbent for controllably selective adsorption of various ionic dyes from aqueous solution by simply adjusting pH, Chem. Eng. J., 382 (2020) 122829.

[45] N.P. Raval, P.U. Shah, N.K. Shah, Adsorptive amputation of hazardous azo dye Congo red from wastewater: a critical review, Environ. Sci. Pollut. Res., 23 (2016) 14810–14853.

[46] I. Langmuir, The adsorption of gases on plane surfaces of glass, mica and platinum, J. Am. Chem. Soc., 40 (1918) 1361–1403.

[47] A. Esmaeili, H. Eslami, Adsorption of Pb(II) and Zn(II) ions from aqueous solutions by Red Earth, MethodsX, 7 (2020) 100804.

[48] B. Royer, N.F. Cardoso, E.C. Lima, J.C.P. Vaghetti, N.M. Simon, T. Calvete, R.C. Veses, Applications of Brazilian pine-fruit shell in natural and carbonized forms as adsorbents to removal of methylene blue from aqueous solutions—kinetic and equilibrium study, J. Hazard. Mater., 164 (2009) 1213–1222.

[49] M. Hasanzadeh, A. Simchi, H.S. Far, Nanoporous composites of activated carbon-metal organic frameworks for organic dye adsorption: synthesis, adsorption mechanism and kinetics studies, J. Ind. Eng. Chem., 81 (2020) 405–414.

[50] G.H. Wang, Z. Zhang, W.B. Li, C.J. Du, T. Chen, Production and characterization of modified biochar by corn cob and its ability to absorb phenol, IOP Conf. Ser.: Mater. Sci. Eng., 729 (2020) 012070.

[51] H.M.F. Freundlich, About the adsorption, Z. Phys. Chem., 57 (1906) 385–470.

[52] M.T. Sultan, H.S. Al-Lami, A.H. Al-Dujiali, Synthesis and characterization of alumina-grafted acrylic acid monomer and polymer and its adsorption of phenol and p-chlorophenol, Desal. Water Treat., 150 (2019) 192–203.

[53] M.J. Tempkin, V. Pyzhev, Kinetics of ammonia synthesis on promoted iron catalysts, Acta Physicochim. URSS, 12 (1940) 217–222.

[54] A. Mellah, D. Harik, Removal pharmaceutical pollutants by adsorption competitive using powdered activated carbon CAP (F400), J. Environ. Treat. Tech., 8 (2020) 336–345.

[55] M. Erdem, E. Yüksel, T. Tay, Y. Çimen, H. Türk, Synthesis of novel methacrylate based adsorbents and their sorptive properties towards p-nitrophenol from aqueous solutions, J. Colloid Interface Sci., 333 (2009) 40–48.